Available online at www.sciencedirect.com
ScienceDirect
Fluid Phase Equilibria 264 (2008) 1–11
FLUID PHASE EQUILIBRIA
www.elsevier.com/locate/fluid

A new equation of state derived by the statistical mechanical perturbation theory

Mohammad Shokouhi, Gholam Abbas Parsafar*

Department of Chemistry, Sharif University of Technology, Tehran, Iran

Received 7 August 2007; received in revised form 2 October 2007; accepted 2 October 2007
Available online 7 October 2007

Abstract

We have derived an analytical equation of state (EOS) based on the soft-core statistical mechanical perturbation theory for fluids, using the Weeks–Chandler–Andersen (WCA) theory recently developed by Ben–Amotz–Stell (BAS) for the choice of the hard-sphere diameter, but with a new algorithm for calculation of the pair and many-body interactions. We have used Carnahan–Starling expression with the Boltzmann factor criterion (BFC) as an effective hard-sphere diameter for the reference system, and also decomposed the perturbed pair potential to symmetric and asymmetric terms. The former term is due to the many-body interactions at high densities as was used in the linear isotherm regularity known as LIR EOS, and the latter term supports the interaction of two isolated particles that is dominating at low densities. The resulting EOS is obtained as $Z = Z_{cs} + \alpha\rho + A\rho^3 + B\rho^5$, in which Z_{cs} is the Carnahan–Starling expression for the compressibility factor of the reference system which contains the effective van der Waals co-volume, and α is due to the asymmetric interaction term, or the attraction contribution of the second virial coefficient. The A and B parameters are the attractive and repulsive contributions of symmetric term, respectively. The temperature-dependencies of all parameters of the EOS are obtained. We select some different fluids, namely Ar, N_2, CH_4, Ne, CO_2, C_2H_6, C_3H_8, NH_3 and H_2O which are spherical, roughly spherical, non-spherical, polar and associated fluids, due to their abundance of P–V–T experimental data. We have found that, except for the critical region, $0.8 < \rho_r \leq 1.5$, $1 \leq T_r \leq 1.5$, the new EOS is accurate for all temperatures and densities available in the literatures, in such a way that the average percent deviation of density for Ar, Ne, N_2, CH_4, CO_2, C_2H_6, C_3H_8, and NH_3 is less than 2.81%. Then some thermodynamic properties including vapor–pressure curve, Joule–Thomson inversion curve, P–T isochors curves, and the second virial coefficient have been applied to check the accuracy of the new EOS. Results for some isochors of argon show that the new EOS gives a small negative curvature for all isochors. The new EOS prediction of the inversion Joule–Thomson curve is reasonable, and its prediction of Clausius–Clapeyron diagram for neon and argon is very accurate, but small deviation for methane and nitrogen can be seen.

Keywords: Equation of state; First-order perturbation theory; Effective hard-sphere diameter; Symmetric and asymmetric interactions

1. Introduction

Over the last decade, the linear isothermal regularity known as the LIR equation of state (LIR EOS) [1] has been extensively used to calculate equilibrium properties of the pure dense classical and metal fluids [2–4]. According to the one-fluid approximation [5], the regularity holds for the dense fluid mixtures as well [6,7]. The LIR is able to predict many experimentally known regularities for pure fluids and fluid mixtures [8–10]. According to the LIR EOS, $(Z-1)\upsilon^2$ is linear with respect to ρ^2 for each isotherm of a fluid for densities greater than the Boyle density and temperatures lower than twice of the Boyle temperature as,

$$(Z-1)\upsilon^2 = A^{LIR} + B^{LIR}\rho^2 \tag{1}$$

where Z is the compressibility factor and $\rho = 1/\upsilon$ is the molar density; A^{LIR} and B^{LIR} are the temperature-dependent parameters, as follows:

$$A^{LIR} = A_2^{LIR} + \frac{A_1}{T} \tag{2a}$$

and

$$B^{LIR} = \frac{B_1}{T} \tag{2b}$$

* Corresponding author. Tel.: +98 21 66165355; fax: +98 21 66005718.
E-mail addresses: Shokouhi@mehr.sharif.edu (M. Shokouhi), Parsafar@sharif.edu (G.A. Parsafar).

0378-3812/$ – see front matter © 2007 Elsevier B.V. All rights reserved.
doi:10.1016/j.fluid.2007.10.002

where A_1 and B_1 are related to the attraction and repulsion terms of the average effective pair potential, respectively, while A_2^{LIR} is related to the non-ideal thermal pressure. This EOS was originally suggested on the basis of a simple lattice-type model applied to the Lennard–Jones (12, 6) fluid [11]. The key point of this equation is related to the mean-field potential that any particle in the system interacts with other particles symmetrically, that we shall refer to it as the symmetric potential, because of uniform distribution of molecules around any given simple spherical molecule at high densities. The shortcoming of Eq. (1) is related to the fact that it does not include the hard-core characteristic of particles explicitly which becomes important at high temperatures, and the asymmetric contribution of the potential which becomes important at low densities (according to which a particle interacts with one or a few particles around it or the clustering effect at low density), and we shall refer to this kind of interaction as asymmetric potential.

The aim of this work is to improve the present EOS to obtain an accurate description of the *P–V–T* behavior and also the equilibrium properties of fluids at the whole density and temperature ranges by recourse of a sound model using a statistical mechanical approach. In this regard we resort to thermodynamic perturbation theory [12], and include symmetric and asymmetric contributions of the pair potential in the perturbation term, then, we use Weeks–Chandler–Andersen (WCA) [13–15] theory for the reference system modified by Ben–Amotz–Stell (BAS) theory [16]. One should notice that the terms "symmetric" and "asymmetric" refer merely to distribution of other molecules around a given molecule, which is uniform in the former case and non-uniform in the latter case. In the case of non-spherical molecules, the unweighted average over the molecular orientation (known as RAM theory [17,18]) may be taken into account to avoid the angular dependence of the potentials. The symmetric contribution is due to the interactions of a given molecule with those that uniformly are distributed around it. Such contribution is the main interaction in a dense fluid. However, in a dilute gas, the nearest neighbors of a given molecule are not distributed around it, symmetrically, especially due to formation of dimmers or other clusters with a few molecules. Such interactions make the asymmetric contribution, which is the major interaction in dilute gases. The minor interaction of a molecule in dilute gas with the farther molecules, which are symmetrically distributed around it, may be considered as the symmetric contribution of the interaction potential. In the following section, we propound a summary of served model, and then we shall derive the new EOS, and using it to calculate some equilibrium properties.

2. Statistical mechanical derivation of the new EOS

For a system of soft-repulsion with added attraction pair potential, the excess free energy (F^{ex}) may, without loss of generality, be expressed as the sum of the free energy of the reference fluid, F_0^{ex}, plus a term representing the difference between the free energy of real and reference systems ΔF,

$$F^{\mathrm{ex}} = F_0^{\mathrm{ex}} + \Delta F \tag{3}$$

The Zwanzig's first-order perturbation theory [19] implies the following expression for ΔF,

$$\frac{\beta \Delta F}{N} = 2\pi\rho\beta \int_0^\infty g_0(r)\, u_1(r) r^2\, \mathrm{d}r \tag{4a}$$

where $g_0(r)$ is the radial distribution function of the reference system, $u_1(r)$ is the potential energy of the perturbed system, and $\beta = 1/k_{\mathrm{B}}T$, where k_{B} is the Boltzmann constant. Barker–Henderson [12] derived Eq. (4a) for the first-order term with another approach. They divided the range of intermolecular distances into interval $(r_0, r_1), \ldots, (r_i, r_{i+1}), \ldots$, etc., by taking the limit as the interval width approaches to zero, the continuous description is recovered. If N_i represents the number of molecules in a spherical shell surrounding a central molecule and $u_1(r)$ be as a constant value of u_i in the spherical shell, the first term of the excess free energy may be given as,

$$\beta \Delta F = \beta \sum_i \langle N_i \rangle u_i, \tag{4b}$$

where,

$$\langle N_i \rangle = 2\pi N \rho \int_i^{i+1} g_0(r) r^2\, \mathrm{d}r$$

For the continuum limit, Eq. (4b) leads to Eq. (4a).

In this work, we decompose the perturbed energy into two terms, the first term is the symmetric potential (u_1^{s}) is the same as that in the LIR EOS, and the second term which is the asymmetric potential ($u_1^{\mathrm{as}}(r)$) which becomes significant at low densities, thus, Eqs. (4a) and (4b) may be written as,

$$\begin{aligned}\frac{\beta \Delta F_1}{N} &= 2\pi\rho\beta \int_0^\infty g_0(r)(u_1^{\mathrm{s}}(r_{\mathrm{av}}) + u_1^{\mathrm{as}}(r)) r^2\, \mathrm{d}r \\ &= \frac{\beta \Delta F_1^{\mathrm{s}}}{N} + \frac{\beta \Delta F_1^{\mathrm{as}}}{N}\end{aligned} \tag{5}$$

where r_{av} is the average distance between the nearest neighbors. $\beta \Delta F_1^{\mathrm{s}}/N$ and $\beta \Delta F_1^{\mathrm{as}}/N$ are the symmetric and asymmetric contributions to the Helmholtz free energy, respectively. The potential energy related to the symmetric contribution as a mean-field interaction potential depends on density and may depends on temperature, but not to the radial distance [20]. By regarding only the first shell in Eq. (4b) we may write,

$$\frac{\beta \Delta F_1^{\mathrm{s}}}{N} = \frac{u_1^{\mathrm{s}}(\rho)\beta \left(4\pi\rho \int_{\text{first shell}} g_0(r) r^2\, \mathrm{d}r\right)}{2} = \beta\, u_1^{\mathrm{s}}(\rho) \frac{z(\rho)}{2} \tag{6}$$

where $z(\rho)$ is the average number of the nearest neighbors. As in the LIR EOS, we approximate the average potential energy by summing contribution from the nearest neighbors' only, assuming Lennard–Jones potential for the effective pair potential,

$$u_1^{\mathrm{s}}(\rho) = \left(\frac{C_{\mathrm{n}}}{r_{\mathrm{av}}^{12}} - \frac{C_{\mathrm{m}}}{r_{\mathrm{av}}^{6}}\right) \tag{7}$$

where C_{n} and C_{m} are constants. We assume that $z(\rho)$ to be proportion to ρ [1], as in the LIR EOS, and $\rho \propto 1/r_{\mathrm{av}}^3$, so that $\beta F_1^{\mathrm{s}}/N$

can be written as,

$$\frac{\beta\Delta F_{\mathrm{I}}^{\mathrm{s}}}{N} = \beta K_{\mathrm{m}}\rho^3 + \beta K_{\mathrm{n}}\rho^5 = \frac{A}{3}\rho^3 + \frac{B}{5}\rho^5 \tag{8}$$

where K_{m} and K_{n} are constants, and $A/3 = \beta K_{\mathrm{m}}$ and $B/5 = \beta K_{\mathrm{n}}$. It is worth noting that, in the LIR EOS, the powers of r_{av} in Eq. (7) had been taken as 3 and 9, and in a recent investigation the values of 6 and 12 were found to be more accurate [21].

The asymmetric term of Helmholtz free energy is assumed to be mainly due to the two body interactions which is valid at low densities, in this case, the radial distribution function of the reference system is approximately equal to $\exp[-\beta u_0(r)]$, so by using Eq. (5), $\beta\Delta F_{\mathrm{I}}^{\mathrm{as}}/N$ may be written as [22],

$$\frac{\beta\Delta F_{I}^{\mathrm{as}}}{N} = 2\pi\rho\beta\int_0^\infty g_0(r)u_{\mathrm{I}}^{\mathrm{as}}(r)r^2\,\mathrm{d}r = 2\pi\rho\beta\int_0^\infty \exp[-\beta u_0(r)]u_{\mathrm{I}}^{\mathrm{as}}(r)r^2\,\mathrm{d}r \tag{9}$$

Eq. (9) equals to the contribution of the perturbation energy due to the second virial coefficient, $B_2(T)$. To show this claim, we may write,

$$B_2(T) - B_2^0(T) = 2\pi\int_0^\infty ((1-\exp[-\beta u(r)]) - (1-\exp[-\beta u_0(r)]))r^2\,\mathrm{d}r \tag{10}$$

By noting that $u(r) = u_0(r) + u_{\mathrm{I}}(r)$, and with expanding the perturbation term, Eq. (10) may be rearranged to,

$$B_2(T) - B_2^0(T) = 2\pi\int_0^\infty (\beta u_{\mathrm{I}}(r))\exp[-\beta u_0(r)]r^2\,\mathrm{d}r \tag{11}$$

As mentioned in reference [23] and is justified by a numerical observation [24], the plot of $\exp[-\beta u_0(r)]$ as a function of r, shows that, it is approximately equals to step function, $\theta(r-\sigma_{\mathrm{HS}}) = \exp[-\beta u_{\mathrm{HS}}(r)]$, so we may conclude that asymmetric term of Helmholtz free energy is roughly expressed by the following equation,

$$\frac{\beta\Delta F_{\mathrm{I}}^{\mathrm{as}}}{N} = (B_2(T) - B_2^0(T))\rho \approx (B_2(T) - b(T))\rho = \alpha\rho \tag{12}$$

The final expression for the full excess Helmholtz free energy is found to be as,

$$\frac{\beta F^{\mathrm{ex}}}{N} = \frac{\beta F_{\mathrm{HS}}^{\mathrm{ex}}}{N} + \alpha\rho + \frac{A}{3}\rho^3 + \frac{B}{5}\rho^5 \tag{13}$$

The compressibility factor associated with Eq. (13) is,

$$Z = \rho\left(\frac{\partial(\beta F/N)}{\partial\rho}\right)_\beta = Z_{\mathrm{CS}} + \alpha\rho + A\rho^3 + B\rho^5 \tag{14}$$

where,

$$Z_{\mathrm{cs}} = \frac{1+\eta+\eta^2-\eta^3}{(1-\eta)^3} \tag{15}$$

where Z_{cs} is Carnahan–Starling (CS) [25] equation of state as the reference system, and η is the packing fraction equal to $(b(T)/4)\rho$, where $b(T)$ is effective vdW co-volume depended on effective hard-sphere diameter (σ_{HS}). The presence of a term linear in density is of general believe in the community that dates back to van der Waals, but one of the significant feature of Eq. (14), like the Prausnitz EOS [26], is that, it is a modification of the original peculiar result, whereby the first-order perturbation gives extra linear terms of order −3 and −5 in the density.

There are some criteria to attribute a value to σ_{HS}, when the equal compressibility criterion is used, it appears to be a function of both temperature and density [27], but we try to use a criterion which has following qualification: (1) to have an analytical form for σ_{HS}, (2) for simplicity to be a function of temperature only. (3) To satisfy Eq. (12) [23,24]. For these reason, we use the Boltzmann factor criterion (BFC) [28], according to which σ_{HS} takes the value of r in such a way that,

$$\beta u_0(r = \sigma_{\mathrm{HS}}) = \xi \tag{16}$$

ζ is a parameter which may varies from 0.5 to 1.5, but owing to the fact that for two molecules moving in a three dimensional space to collide at any time, their velocity vectors must lie on the same plane, hence in this work, we have considered $\zeta = 1$. Thus, effective vdW co-volume obtained with the Lennard–Jones (LJ),

$$b(T) = \frac{2\pi}{3}N_0\sigma_{\mathrm{HS}}^3 = \frac{2\pi}{3}N_0\sigma^3\left[\frac{2}{1+(\zeta/\beta\varepsilon)^{0.5}}\right]^{0.5} \tag{17}$$

where N_0 is the Avogadro constant. Owing to this fact, the second virial coefficient can be written as a power series in terms of reciprocal of temperature which may be derivable from arbitrary potential model, by using Eq. (12). Note that the BFC criterion has extensively been used by BAS perturbation theory [16].

Temperature-dependencies of α (asymmetric contribution to the potential) may generally be written as a power series in terms of $1/T$.

$$\alpha(T) = (B_2(T) - b(T)) = \frac{\alpha_1}{T} + \frac{\alpha_2}{T^2} + \frac{\alpha_3}{T^3} + \cdots \tag{18}$$

Temperature-dependencies of the parameters which are related to the symmetric potential are as the LIR EOS,

$$A = \frac{A_1}{T} = 3\beta K_{\mathrm{m}}, \qquad B = \frac{B_1}{T} = 5\beta K_{\mathrm{n}} \tag{19}$$

Note that in the LIR $A = A_2 + A_1/T$, where A_2 is the contribution due to the non-ideal thermal pressure, which is more accurately included in both Z_{CS} and the asymmetric contribution in this work. The derived EOS has four scaling parameters, namely effective van der Waals co-volume, $b(T)$, which is temperature-dependent, a new parameter which is contribution of the attractive pair potential to the second virial coefficient, $\alpha(T)$, which denotes the asymmetric effects of the internal energy, both can be derived from the molecular parameters such as potential well (ε) and the distance where the potential function becomes zero (σ). Two other scaling parameters are the attractive (A) and repulsive (B) contributions of the effective pair potential of the many-body interactions, which we denote the symmetric effects of the internal energy. Since we have not any insight about the molecular parameters-dependency into the scaling factors (A, B), we have obtained all scaling parameters by

fitting experimental P–V–T data into Eq. (14). Owing to the fact that Z_{cs} and $\alpha(T)$ have two and three fitting parameters, respectively, therefore Eq. (14) has totally seven fitting parameters, all of which have physical interpretations.

3. Experimental test

To examine the accuracy of the derived EOS, Eq. (14), we serve argon as our primary test fluid because of the abundance of available P–V–T data. The deviation curves of density for some typical non-critical isotherms including subcritical, and supercritical isotherms are shown in Fig. 1a, where it can be seen that experimental data are well fitted onto Eq. (14). Average deviation for all isotherms except for the critical and near critical ones are less than 2% which is reasonable, however, around the critical point ($T_C = 150.69$ K, $\rho_c = 13.407$ mol/l), the deviation is significantly larger. The deviation curves for the critical and its higher temperature isotherms are shown in Fig. 1b, according to which the deviation in the critical region, $1 \le T_r \le 1.5$ and $0.8 \le \rho_r \le 1.5$, is significant ($T_r = T/T_C$, $\rho_r = \rho/\rho_c$). The results of fitting are summarized in Table 1, including the scaled parameters, pressure range of experimental data, coefficient of determination, and the average and maximum percent deviations of the calculated density for some isotherms. Also, the results for some temperatures are compared to those of Soave–Redlich–Kwong [29] and Deiters [30] EOSs, for which the results are listed in Table 2. To see whether the new EOS is limited to certain type of fluids, similar calculations are done for other fluids including Ne, Ar and CH_4 (spherical molecule), N_2 (diatomic molecule), CO_2 (linear molecule), C_2H_6, C_3H_8 and *iso*-C_4H_{10} (non-spherical molecules) and also polar molecules NH_3 and H_2O are served, for which the results are summarized in Table 3. It should be pointed out that the experimental P–V–T data are taken from references [31] and [32]. Note that for the fluids listed in Table 3, except for water, the calculated values of ρ are relatively accurate in comparison with experimental data. As may be seen in Table 3 the coefficient of determination of water becomes lower at low temperatures which may be due to the hydrogen bond formation. In water, hydrogen bonds lead at low temperatures to the formation of an open, approximately four-coordinated structure, in which entropy and density decrease with decreasing temperature, and thereby we need a suitable models which includes this effect [33,34]. Deviation curves against the reduced density for four isotherms of water are shown in Fig. 2, as seen for $T_r = 1.159$ there are remarkable deviations around the critical density, but for $T_r = 1.97$, the deviation is low.

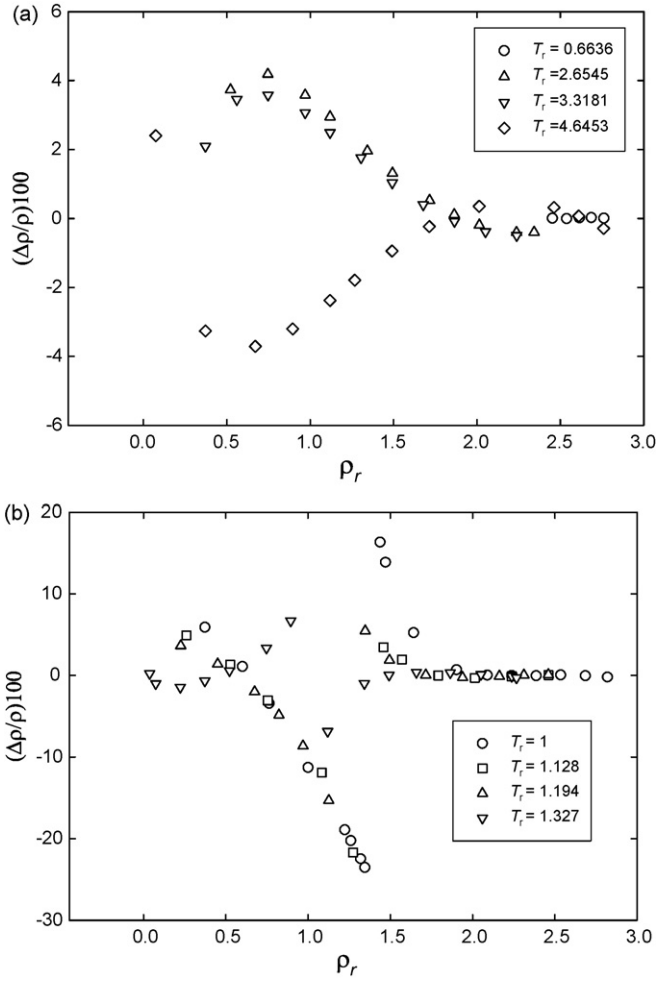

Fig. 1. Deviation curve of density for some (a) non-critical and (b) critical and near critical isotherms of argon.

Table 1
The parameters of the EOS obtained from fitting P–V–T experimental data into Eq. (14), along with the pressure range of experimental data ΔP, coefficient of determination R^2, and average (maximum) percent deviation of the calculated density for some given isotherms of argon

T/T_C	$b(T) \times 10^3$ (l/mol)	$\alpha(T) \times 10^2$ (l/mol)	A ($\times 10^5$) (l/mol)^3	B ($\times 10^8$) (l/mol)^5	R^2	ΔP (MPa)	$100(\lvert\Delta\rho\rvert/\rho)_{av}$ [a]
0.6636	52.6900	−19.6168	−7.8632	2.09284	0.9999	0–68	0.007 (0.017)
1.0000	50.0863	−12.7783	−5.24211	1.39523	0.9997	0–250	8.020 (23.60)
1.1281	49.2576	−11.29548	−4.62539	1.23108	0.9988	0–435	4.40 (15.70)
1.1945	48.8759	−10.66455	−4.36842	1.16269	0.9988	0–465	3.36 (10.3)
1.3272	48.1672	−9.58882	−3.93158	1.04642	0.9980	0–600	2.54 (8.80)
1.9908	45.3906	−6.55358	−2.62105	0.69761	0.9988	0–1000	1.80 (5.20)
2.6545	43.3889	−4.72889	−1.96579	0.52321	0.9990	0–1000	1.76 (4.18)
3.3181	41.8287	−3.66707	−1.57263	0.41857	0.9990	0–1000	1.68 (4.00)
4.6453	39.4793	−2.42779	−1.12331	0.29898	0.9998	0–1000	1.53 (3.71)
5.3089	38.5520	−2.07113	−0.982895	0.261605	0.9998	0–1000	0.90 (1.94)
6.6361	37.0138	−1.60529	−0.786316	0.209284	0.9997	0–1000	0.85 (1.85)

[a] The maximum percent deviation is given in the parentheses.

Table 2
The percent average absolute deviation of density of the new EOS compared to those of Soave–Redlich–Kwong [29] and Deiters [30] EOSs

T/T_C	$\Delta\rho$ (mol/l)	This work[a] $(\lvert\Delta\rho\rvert/\rho)\times 100$	SRK[a] $(\lvert\Delta\rho\rvert/\rho)\times 100$	Deiters[a] $(\lvert\Delta\rho\rvert/\rho)\times 100$
0.5641	32.9–38.0	0.05 (0.06)	0.86 (0.98)	0.07 (0.10)
0.6636	35.3–37.0	0.107 (0.137)	1.10 (1.64)	1.10 (1.49)
1.9908	1.0–35.0	1.80 (5.20)	14.35 (69.1)	10.84 (41.30)
4.6453	1.0–38.5	1.53 (3.71)	3.42 (8.33)	7.56 (13.50)

[a] The maximum percent deviation is given in the parentheses.

Table 3
Same as Table 1 for some different fluids

Fluid	T/T_C	$b(T)\times 10^3$ (l/mol)	$\alpha(T)\times 10^2$ (l/mol)	A $(\times 10^5)$ $(\text{l/mol})^3$	B $(\times 10^8)$ $(\text{l/mol})^5$	R^2	ΔP (MPa)	$100(\lvert\Delta\rho\rvert/\rho)_{av}$[a]
Ne	0.787	30.7390	−9.1654	−1.47988	3.577×10^{-4}	0.9998	0–80	0.06 (0.1)
Ne	6.743	21.5968	−1.1022	−0.17265	4.140×10^{-5}	1.000	0–571	0.25 (2.00)
Ne	15.733	18.5907	−0.5175	−0.073994	1.774×10^{-5}	1.000	0–700	0.08 (0.55)
CH_4	0.787	63.7280	−23.6821	−5.70205	9.91856	0.9998	0–250	0.75 (1.20)
CH_4	3.149	51.7290	−3.8660	−1.42550	2.47964	0.9995	0–1000	2.50 (6.50)
N_2	0.713	58.3360	−22.8821	−10.1650	11.08710	0.9995	0–145	0.48 (0.86)
N_2	5.547	43.0848	−1.0407	−1.3070	1.42548	0.9993	0–900	2.3 (8.90)
N_2	10.302	38.4240	−0.3123	−0.70378	0.767567	0.9995	0–1500	2.81 (5.40)
N_2	15.849	35.3020	−0.1289	−0.45745	0.49892	0.9992	0–2200	1.70 (3.00)
C_2H_6	0.655	104.5520	−36.000	−93.1877	93.44360	0.9998	0–140	0.06 (0.10)
C_2H_6	2.620	91.4350	−9.2636	−23.2970	23.36100	0.9997	0–140	0.37 (0.70)
C_3H_8	0.541	149.4218	−61.7660	−290.440	276.8100	0.9998	0–205	0.10 (0.15)
C_3H_8	2.163	134.1534	−16.2176	−72.6100	69.20220	0.9998	0–205	1.20 (3.00)
CO_2	0.904	65.4419	−18.3616	−12.3402	1.2748	0.9997	0–100	0.60 (0.90)
CO_2	3.617	53.4463	−3.1005	−3.0850	0.31870	0.9995	0–1141	2.65 (8.10)
NH_3	0.740	42.2459	−16.6115	−0.55122	0.45073	0.9997	0–60	0.24 (0.30)
NH_3	1.723	37.4991	−5.8625	−0.23624	0.19370	0.9999	0–1000	1.00 (5.95)
H_2O	0.618	29.3949	−12.4016	−0.144366	0.12621	0.9984	0–1000	0.56 (0.80)
H_2O	0.773	28.8034	−10.3454	−0.115493	0.10097	0.9985	0–1000	0.3 (0.75)
H_2O	1.159	27.1802	−6.5853	−0.076995	0.06731	0.9987	0–1000	5.06 (18.35)
H_2O	1.39	26.2900	−5.1838	−0.064163	0.05609	0.9996	0–1000	4.3 (17.80)
H_2O	1.970	24.4156	−3.1021	−0.045291	0.03960	0.9998	0–1000	2.27 (7.03)

Average percent deviation for isotherm of any fluid is less than 2.81%, except for the low temperature supercritical of water.
[a] The maximum percent deviation is given in the parentheses.

Not surprising that, the worst agreement appears around the critical point. The average absolute percent deviation, except for the critical region for Ne is about 0.25, for Ar 1.8%, for CH_4 2.5%, for N_2 2.81%, for CO_2 2.65%, for NH_3 1.0%, for C_2H_6 and C_3H_8 are less than 1.2%.

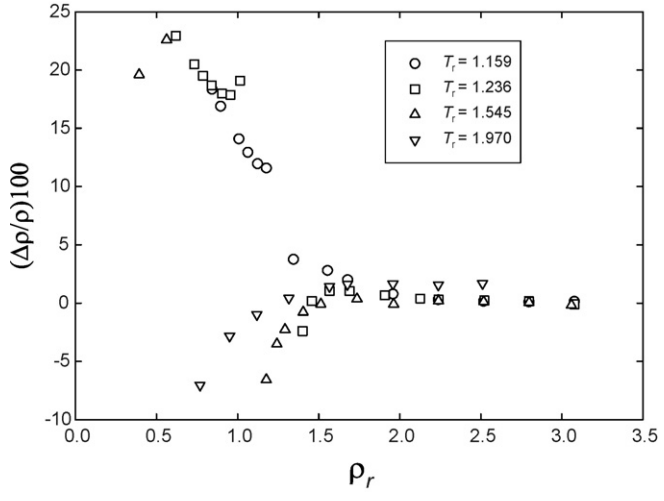

Fig. 2. Deviation curves of density for T_r = 1.159, 1.236, 1.545 and 1.97 of water.

3.1. Temperature-dependencies of the parameters

In Section 2, we presented a model for temperature-dependencies of the scaled parameters of the EOS; here, we test the derived model for argon to investigate the temperature-dependencies of the scaled parameters. On the basis of Eqs. (14)–(19), A and B are proportion to the reciprocal of temperature, and $\alpha(T)$ is a power series in terms of $1/T$ which may be truncated after the third term, and $b(T)$ is derived by the BFC criterion which obeys Eq. (17). But for a general case we may use the BFC expression obtained with the generalized Lennard–Jones (GLJ) rather than LJ. The effective co-volume for the GLJ model is like that of Eq. (17), but the exponent 0.5 is replaced by $6/n_0$, where n_0 is an exponent that characterizes the steepness of the GLJ repulsive branch [35].

The values of the scaled parameters given in Table 1 for argon are used to check the predictions of temperature-dependencies of the model. In Fig. 3 temperature-dependencies of the obtained adjustable parameters of argon given in Table 1 for some different isotherms are fitted into the predicted expressions, Eqs. (17)–(19). As seen in these figures, the fittings are well done, with $R^2 = 1.000$ for A and B, $R^2 = 0.9997$ for $\alpha(T)$ and $R^2 = 1.000$

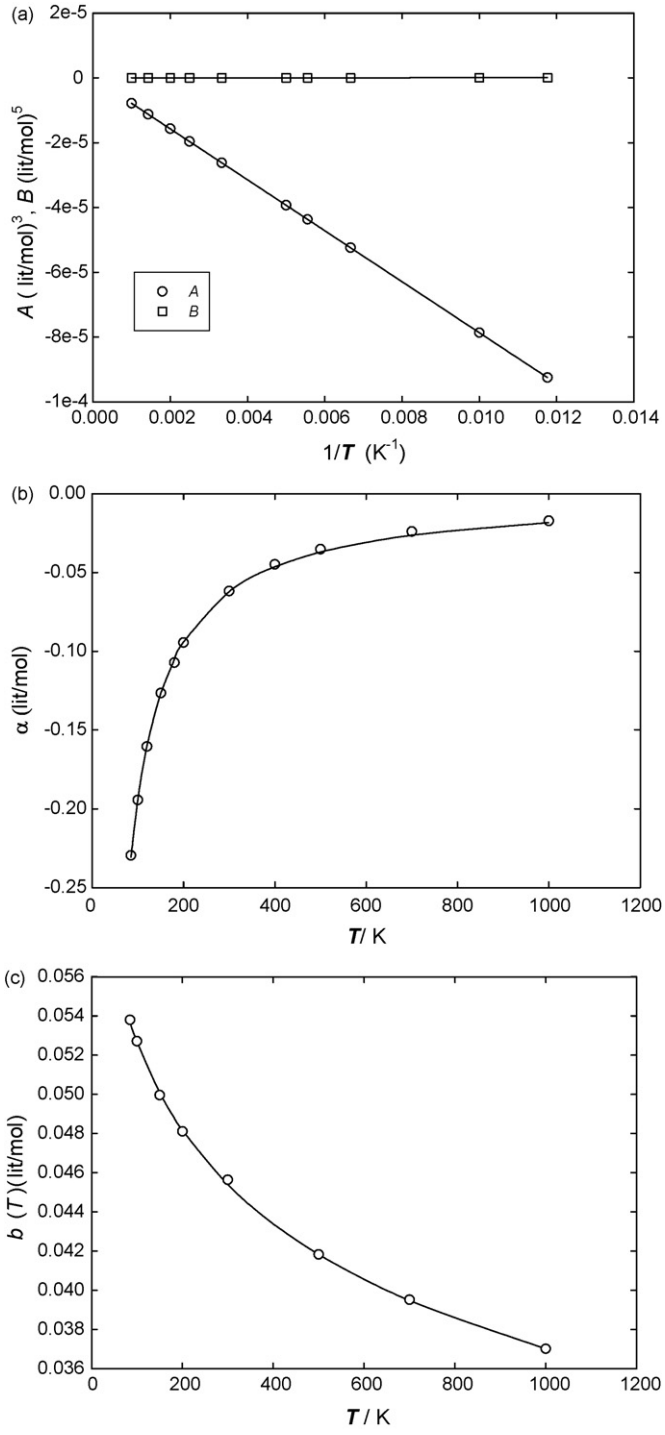

Fig. 3. The temperature-dependencies of (a) symmetric parameters of new EOS With $R^2 = 1.000$, (b) asymmetric parameter with $R^2 = 0.9997$, and (c) effective vdW co-volume which is fitted into the BFC criterion with $\zeta = 1$, $R^2 = 1.000$ for argon.

for $b(T)$. We have used Eqs. (18) and (19) to obtain five temperature-independent constants, namely α_1, α_2, α_3, A_1, and B_1. To do so, the data for A, B, and α at some different temperatures are needed which may be obtained by fitting experimental P–V–T data to the EOS. The values are given in Table 4a for some given fluids.

3.2. Calculation of the potential parameters

The values of effective co-volumes $b(T)$ for some fluids used in this work are fitted into Eq. (17), to obtain the pair potential parameters for them which may be compared with the corresponding LJ parameters obtained from the second virial coefficient data [36a], which are listed in Table 4b. As may be seen the calculated parameters are comparable to those of the LJ potential. As shown in this Table, the value of b_0 depends on product of ε/k and $1/\zeta$ to which ε/k is inversely proportional.

4. Comparison with the LIR at high densities

The rearrangement of the new EOS in the form of LIR EOS may be written as,

$$(Z-1)\upsilon^3 = \frac{1}{\rho^3}\left(\frac{4\eta - 2\eta^2}{(1-\eta)^3} + \alpha\rho\right) + A + B\rho^2 = \left(A_2 + \frac{A_1}{T}\right) + \left(\frac{B_1}{T}\right)\rho^2 \tag{20}$$

for which,

$$A_2 = \frac{1}{\rho^3}\left(\frac{4\eta - 2\eta^2}{(1-\eta)^3} + \alpha\rho\right) \tag{21}$$

where A_2 is the non-ideal thermal pressure. On the basis of van der Waals EOS and also using experimental data, it was assumed that A_2 is almost a constant at high density [1]. Such an assumption may be investigated from Eq. (21). The results for 4 isotherms of argon are shown in Fig. 4. As may be seen, at high densities the values of A_2 are approximately independent of density. Therefore, one may conclude that non-ideal thermal pressure is almost constant only at high densities. As can be seen from the expression for A_2, Eq. (21), it depends on both the asymmetric parameter $\alpha(T)$ and vdW co-volume $b(T)$. The significant density-dependence of A_2 at low densities is expect to be due to the asymmetric parameter of intermolecular interactions, $\alpha(T)$. From the high-density behavior of the new EOS, we may draw some conclusions; first the linear regime of $(Z-1)\upsilon^3$ versus ρ^2 does not depend on any special feature of the molecular interaction but only on the existence of long range attraction and short range repulsion, due to the generality for all type of fluids. These results have been also pointed out, based on the vdW and Ihm–Song–Mason (ISM) EOSs in reference [1]. Careful inspection at high densities, as shown in the sub-portion of Fig. 4, A_2 varies slightly by temperature and density whose functionalities are shown elsewhere [37,38]. Temperature-dependencies of A_2 is important because in the case of its temperature-independencies, two common intersection points (namely, the common bulk modulus and common compression point) were found to be independent of temperature [8], whereas according to experimental data, they slightly change with temperature [39].

Table 4a
Temperature-independent parameters of some fluids

	α_1 ($K l^{-1} mol^{-1}$)	α_2 ($K^2 l^{-1} mol^{-1}$)	α_3 ($K^3 l^{-1} mol^{-1}$)	A_1 ($K l^{-3} mol^{-3}$) × 10^3	B_1 ($K l^{-5} mol^{-5}$) × 10^6
Ar	−17.682508	−353.52571	15442.104	−7.8631587	2.0928419
Ne	−3.4098826	11.601395	−150.0371	−0.5179569	0.000125200
N_2	−8.8474498	−1623.3519	51898.136	−9.1908960	9.9783740
CO_2	−26.760025	−9608.663	857538.91	−33.935572	3.50569221
CH_4	−21.271528	−3188.5403	152696.83	−8.5530705	14.877840
NH_3	−24.927739	−12182.448	1162270.5	−1.6536690	1.3521921

Table 4b
Potential parameters obtained from temperature-dependencies of the effective der Waals co-volume, Eq. (17), compared to the LJ values obtained from the second virial coefficient

	This work		LJ	
	$\varepsilon/k\zeta$ (K)	$b_0 \times 10^3$ (l/mol)	ε/k (K)	$b_0 \times 10^3$ (l/mol)
Ar	122.4500	51.4060	122.0	49.58
CH_4	130.0000	64.8990	148.0	70.16
N_2	118.200	56.4474	95.90	64.42
Ne	31.1100	31.1034	34.90	27.10
CO_2	298.0000	64.6943	205.0	85.05
NH_3	116.3000	48.8700	–	–

5. Accuracy of the new EOS in predicting thermodynamics properties of fluids

In this section we give a selection of some properties, and test the new derived EOS, which includes the second and third virial coefficients, linearity of isochors, Joule–Thomson inversion curve, two-phase region (co-existence curve), and Clausius–Clapeyron curve.

5.1. Second and third virial coefficients

At the zero density limit, expansion of Eq. (14) gives an infinite series in terms of density as,

$$Z = 1 + (b(T) + \alpha(T))\rho + \tfrac{5}{8}(b(T)\rho)^2 + \tfrac{9}{32}(b(T)\rho)^3 + \tfrac{7}{64}(b(T)\rho)^4 + \cdots + A\rho^3 + B\rho^5 \quad (22)$$

where R is the molar gas constant. According to Eq. (22), the second virial coefficient equals to,

$$B_2(T) = b(T) + \alpha(T) \quad (23)$$

which may also be derived from Eq. (18). In Fig. 5, we have shown the calculated second virial coefficient versus temperature for Ar and N_2, compared to experimental value. This figure shows that Eq. (23) predicts the second virial coefficient with a reasonable precision at least qualitatively for simple fluids, since it contains both repulsive and attractive contributions to the calculated second virial coefficient. It is worth noting because of the fact that the effective van der Waals co-volume is temperature-dependent, in accordance with Eq. (17), the calculated second virial coefficient by Eq. (23) would pass through a maximum (very smoothly) at the inversion temperature [40,41]. Owing to the fact that applicability of LIR EOS is limited to densities greater than the Boyle density; the second virial coefficient which is due to the pair interactions is irrelevant.

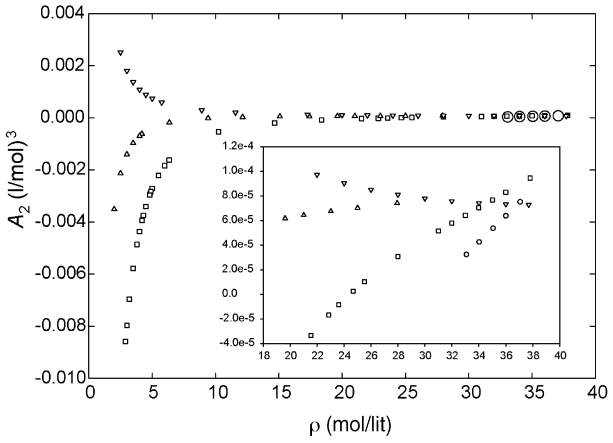

Fig. 4. Temperature and density-dependencies of non-ideal thermal pressure for 100 K (◯), 150.69 K (□), 300 K (△), 700 K (▽) isotherms of Ar.

The third virial coefficient given by the EOS is monotonically decreasing function of T and positive. This is obviously an incorrect prediction at low temperatures, at which the higher virial coefficients are negative [42]. The reason for such incorrect prediction is that, the clusters with more than two particles are not included in deriving the EOS.

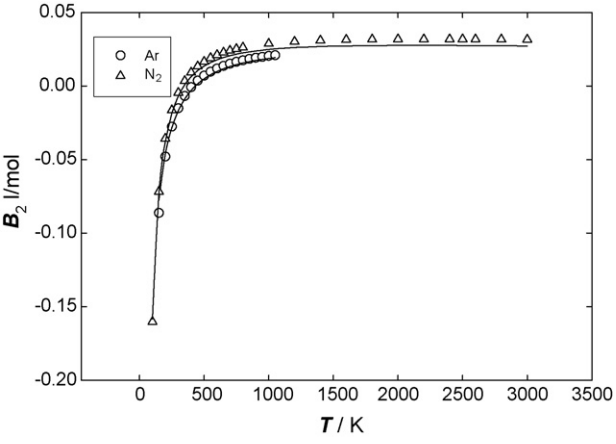

Fig. 5. The calculated second virial coefficient versus temperature using new Eq. (23) in comparison with experimental data for Ar (◯) and N_2 (△).

5.2. P–T isochors

The earliest investigators of fluid compressibility were impressed by the fact that the curves of constant density in a *P–T* plot were nearly linear for real fluids [43], thus a sensible EOS must give nearly linear isochors. Although by further inspection, it was found that the isochors of real fluids show slightly negative curvatures (concave downward) at both low and high densities except for some hydrocarbons that show a region of small positive curvature. The isochors of the van der Waals EOS are all linear, but those of the Dieterci EOS all show a positive curvature, and those of the Beattie–Bridgeman and Redlich–Kwong EOSs all show a negative curvature. Some other EOSs like Benedict–Webb–Rubin, isochors show a shift from negative to positive and back to a negative curvature as density increases. The Song–Mason [44] EOS for the LJ (12, 6) fluid shows a small negative curvature for all isochors, and on the basis of Eq. (1), pressure versus temperature for any isochor is linear according to the LIR, just like van der Waals EOS. Our results for argon diagrammatically are shown for a number of isochors in Fig. 6, and compared with experimental data. As may be seen from this figure, all isochors show a small negative curvature, just like ISM EOS and experimental data. It is interesting to note that the departure from the linearity is promoted by both the intermolecular attractions and temperature dependencies of hard-core repulsions.

5.3. The Joule–Thomson inversion curve

The Joule–Thomson inversion curve (JTIC) is the locus of thermodynamic states on which the temperature of system does not vary with isenthalpic expansion or the locus of points at which the Joule–Thomson coefficient is zero. This curve has been proposed as a very sensitive test of equation of state [2,45,46]. It is related to the EOS by the following thermodynamic expression,

$$\mu_{\mathrm{JT}} = \left(\frac{\partial T}{\partial P}\right)_H = \frac{1}{C_P}\left(T\left(\frac{\partial V}{\partial T}\right)_P - V\right) = 0 \tag{24}$$

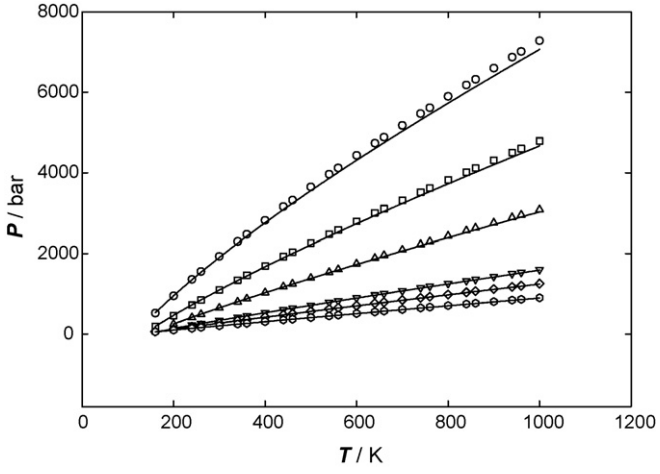

Fig. 6. Pressure–temperature diagram for 30.04 mol/l (◯), 25.03 mol/l (□), 20.026 mol/l (△), 13.407 mol/l (▽), 11.265 mol/l (◇), 8.7614 mol/l (⬡) isochors of Ar, compared to experimental values.

where C_P is the heat capacity at constant pressure. The JTIC may be alternatively characterized by any of the following expressions:

$$T\left(\frac{\partial P}{\partial T}\right)_\rho - \rho\left(\frac{\partial P}{\partial \rho}\right)_T = 0, \qquad \left(\frac{\partial V}{\partial T}\right) = \frac{V}{T}$$
$$\left(\frac{\partial Z}{\partial T}\right)_P = 0, \qquad \left(\frac{\partial Z}{\partial V}\right)_P = 0 \tag{25}$$

Gunn et al. [47] obtained a generalized inversion curve using the volumetric data for some spherical and semi-spherical fluids, and determined the following expression by a least-square curve fit of 89 inversion points obtained from experimental inversion-point data,

$$P_{\mathrm{r}} = -36.275 + 71.598T_{\mathrm{r}} - 41.567T_{\mathrm{r}}^2 + 11.826T_{\mathrm{r}}^3 - 1.6721T_{\mathrm{r}}^4 + 0.091167T_{\mathrm{r}}^5 \tag{26}$$

where P_{r} and T_{r} are the reduced pressure and reduced temperature, respectively. Since the substances used in the correlation have a value of acenteric factor close to zero, the correlation is limited to simple fluids such as Ar, Ne, CH_4 and N_2. This fit of experimental JTIC data may be used as a basis for evaluating the accuracy of any EOS [47]. It must be pointed out that Eq. (26) is referred to as an experimental data in literature [46,48]. In reference [46] the JTIC for some cubic EOS (such as Redlich–Kwong, Soave–Redlich–Kwong [29] and van der Waals), and also Deiters [30], LIR and modified LIR equations of state were investigated, and shown that except for Deiters EOS, none of them can predict the upper temperature branch with a reasonable accuracy. The Joule–Thomson inversion curve, for argon, methane, nitrogen, and neon are calculated by using the new EOS and schematically shown in Fig. 7. As can be seen from this figure, the new EOS shows a reasonable JTIC for all mentioned fluids, in comparison with Eq. (26).

5.4. Co-existence curve

The Helmholz free energy F is a fundamental thermodynamic function for description of the equilibrium thermodynamic sys-

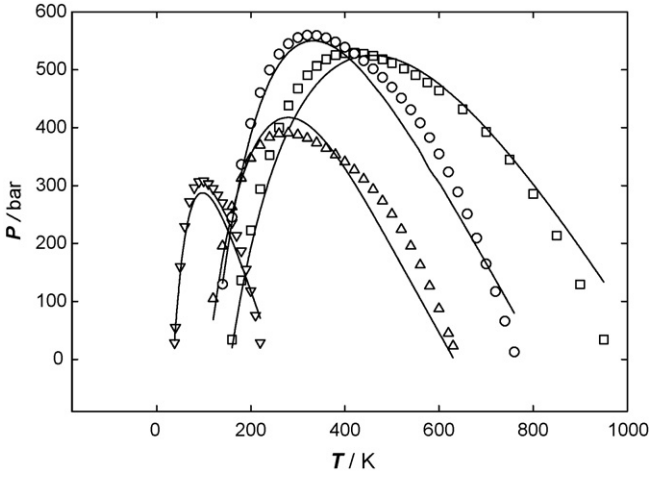

Fig. 7. The calculated Joule–Thomson inversion curve using new EOS compared to Eq. (26) for Ar (◯), CH_4 (□), N_2 (△), and Ne (▽).

tem. By considering changes in V, N and T as principle variables, we may write stability criteria for such a system as [49],

$$\left(\frac{\partial^2 F}{\partial V^2}\right)_{T,N} \geq 0, \qquad \left(\frac{\partial^2 F}{\partial N^2}\right)_{T,V} \geq 0, \tag{27}$$

Since $(\partial F/\partial V)_{T,N} = -P$, it also follows that $\kappa_T = -(1/V)(\partial V/\partial P)_{T,N} \geq 0$.

Stability criteria involving the temperature-dependence of F follows from the energy condition as [49],

$$\left(\frac{\partial S}{\partial T}\right)_{V,N} \geq 0, \tag{28}$$

Since $S = -(\partial F/\partial T)_{V,N}$, we obtain $(\partial^2 F/\partial^2 T) \leq 0$. Obviously F must be a convex-down function in the F–V and F–N planes, but a concave-down function in F–T plane. Michels et al. [50] shown the behavior of the Helmholz free energy isotherms of argon calculated from Peng–Robinson EOS in terms of volume which fails in the two-phase region, because it dose not satisfy the stability criteria condition of Eq. (27), then to have a stable system, fluid breaks down into two phases which its characterization may be determined by the tangent construction from the following condition,

$$\left(\frac{\partial F}{\partial V}\right)_{N,T}\Bigg)_{\mathrm{g}} = \left(\frac{\partial F}{\partial V}\right)_{N,T}\Bigg)_{\mathrm{l}} = \frac{F(V_{\mathrm{g}}) - F(V_{\mathrm{l}})}{V_{\mathrm{g}} - V_{\mathrm{l}}} \tag{29}$$

Eq. (29) shows the conditions from which one may obtain the volumes or densities of the co-existence curve. We have applied Eq. (29) to the new EOS to obtain the density of the co-existence curve, for which the results for four different fluids are shown in Fig. 8.

5.5. Clausius–Clapeyron diagram

In the two-phase region, for any isotherm, we may express the equilibrium conditions as,

$$\mu_{\mathrm{g}} = \mu_{\mathrm{l}}, \qquad P_{\mathrm{g}} = P_{\mathrm{l}} = P_{\mathrm{s}} \tag{30}$$

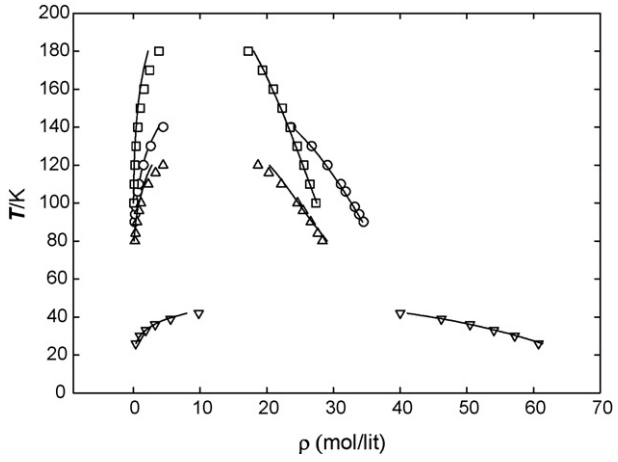

Fig. 8. Co-existence curve calculated by using new EOS compared to experimental data for Ar (◯), CH_4 (□), N_2 (△), and Ne (▽).

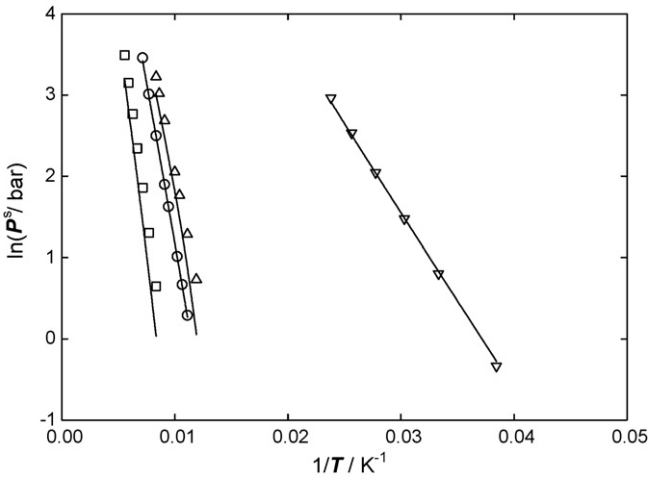

Fig. 9. Clausius–Clapeyron diagram calculated using new EOS compared to experimental data for Ar (◯), CH_4 (□), N_2 (△), and Ne (▽).

where μ_{g} and μ_{l} are the chemical potential of the gas and liquid phases, respectively, and P_{g} and P_{l} are their pressures which both are equal to the saturation pressure, P_{s}.

The Maxwell equal-area construction for an isotherm of Eq. (14) yields the following expression for the saturation pressure,

$$\frac{P_{\mathrm{s}}}{RT}\left(\frac{1}{\rho_{\mathrm{g}}} - \frac{1}{\rho_{\mathrm{l}}}\right) = \left(\frac{\eta(4-3\eta)}{(1-\eta)^2}\right)_{\mathrm{g}}^{\mathrm{l}} + \alpha(\rho_{\mathrm{l}} - \rho_{\mathrm{g}}) + \frac{A}{3}(\rho_{\mathrm{l}}^3 - \rho_{\mathrm{g}}^3) + \frac{B}{5}(\rho_{\mathrm{l}}^5 - \rho_{\mathrm{g}}^5) + \ln\left(\frac{\rho_{\mathrm{l}}}{\rho_{\mathrm{g}}}\right) \tag{31}$$

The vapor–pressure curve known as the Clausius–Clapeyron diagram for four different fluids are shown in Fig. 9.

5.6. Common intersection point of compressibility factor

There is a common compressibility point at which the compression factor against density for different isotherms of any dense fluid intersects at that single point. This intersection point is called a common compression point. The three-shell modification of the Lennard–Jones and Devonshire EOS [36] and also LIR predict the common compression point. The density at this point ρ_{OZ} can be obtained by setting $(\partial Z/\partial T)_{\rho_{\mathrm{OZ}}}$ equal to zero. By the fact that the non-ideal thermal contribution in LIR EOS is temperature-independent, the density at this point is also temperature-independent, $\rho_{\mathrm{OZ}} = A_1/B_1$. We have used the new EOS to calculate the compressibility factor in terms of density for different isotherms. The results are shown for three different isotherms of argon in Fig. 10. As shown in this figure, the new EOS predicts a common intersection point around $\rho_{\mathrm{oz}} = 41$ mol/l, which is comparable with those obtain from experimental data and LIR EOS [8].

5.7. Isochoric heat capacity

Constant volume heat capacity (C_V) is the slope of the internal energy due to random motion of atoms in a sample as a function

Table 5
Calculated critical parameters obtained from the new EOS compare to experimental values for some given fluids

Fluid	Calculated values				Experimental data			
	T_C (K)	ρ_c (mol/l)	P_c (bar)	Z_c	T_C (K)	ρ_c (mol/l)	P_c (bar)	Z_c
Ar	160.06	12.69	59.41	0.36	150.69	13.4074	48.63	0.29
CH_4	212.00	9.29	58.75	0.36	190.54	10.1390	45.99	0.29
N_2	133.21	10.64	43.21	0.37	126.19	11.1839	33.96	0.29
Ne	46.54	22.78	31.39	0.36	44.49	23.8820	26.79	0.30
CO_2	311.80	10.14	93.94	0.36	304.13	10.6249	73.77	0.27

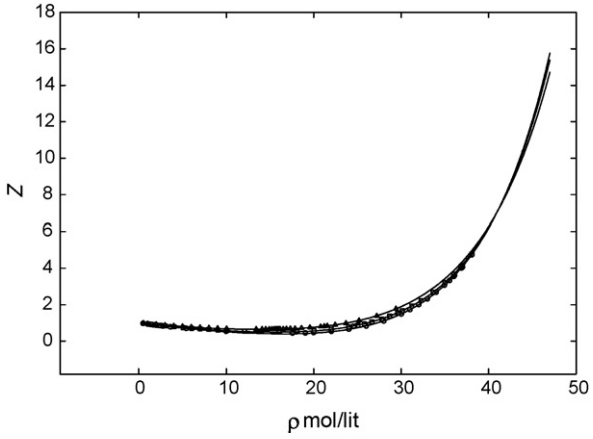

Fig. 10. Ability of the new EOS in predicting a common intersection point for 170 K (◯), 180 K (□), 200 K (△) isotherms of argon.

of temperature, which measured at constant volume. Also, heat capacity may be used as a criterion for the accuracy of an EOS. We may use the following expression to calculate the isochoric heat capacity,

$$\frac{C_V}{Nk} = -\beta^2 \frac{\partial^2}{\partial \beta^2}\left(\frac{\beta F}{N}\right) \tag{32}$$

By using Eqs. (13) and (32) we have calculated C_V on the basis of the new EOS. The results for four deferent isochors are given in Fig. 11. As shown in this figure, the trend of variation of C_V with temperature is the same as the experimental data.

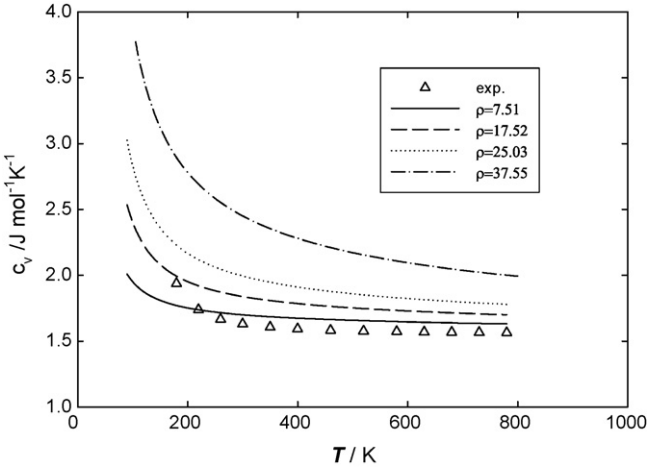

Fig. 11. Calculated constant volume heat capacity for some given isochors of argon. Experimental values for $\rho = 7.51$ mol/l.

5.8. Compressibility factor at the critical point

The critical isotherm appears with its characteristic inflection point, at a point which the first and second volume derivatives of pressure become zero. The critical parameters such as temperature, density, pressure, and compressibility factor obtained from the new EOS are compared with their experimental values in Table 5 for some given fluids.

6. Discussion and conclusion

A new analytical EOS based on the statistical–mechanical perturbation theory is derived for fluids, using the soft-core thermodynamic perturbation theory used Carnahan–Starling expression with the effective diameter as a reference system, but with a new algorithm for taking into account the perturbed potential and thereby a modification amounts to an extra term linear in the density on the first-order perturbation term. We had included the symmetric interaction that a particle sees via all its neighbors as in the LIR EOS, and then derived a new general EOS with a good approximation for whole density and temperature ranges, as shown in Table 2. It is reasonable for non-associating molecules especially for spherical fluids which with high accuracy obey the CS EOS for the reference system and the BFC criterion for effective hard-sphere co-volume.

On the basis of Eq. (21), one may conclude that the non-ideal thermal pressure depends on both hard-sphere characteristic and also asymmetric contribution of molecular interactions which both of them are discarded in the LIR EOS, and such discarding make the application of the LIR limited to the high densities ($\rho \geq \rho_B$) and low temperatures ($T \leq 2T_B$). As shown in Fig. 4, non-ideal thermal pressure (A_2) at low densities deviates significantly from a constant value.

The resulting EOS shows some thermodynamic properties with a reasonable accuracy, such as P–T isochors, as shown in Fig. 6, all isochors show a negative curvature just like experimental data, and because of temperature-dependencies of the hard-sphere diameter, it shows an accurate behavior of the second virial coefficient (see Fig. 5), at least qualitatively, and it predicts the JTIC and also two-phase region diagram with a reasonable accuracy. Some limitations of the new EOS are in order; there are not any molecular insights regarding the symmetric interaction, and it is the reason that we treat them as

adjustable parameters by fitting the experimental P–V–T data into the EOS. Due to the long-range interactions and formation of large clusters at the reduced temperatures and densities range within $1 \leq T_r \leq 15$ and $0.8 \leq \rho_r \leq 15$ (see Table 1 and Fig. 1b), Eq. (14) shows a significant deviation which is expected from the mean-field theory, but at the reduced temperatures higher than 1.5, existence of such clusters can be neglected, because particles convey high kinetic energies. Its applicability is doubtful for substances like H_2O for which the attractive rather than the repulsive interaction plays an important role on the structure of liquid especially at low temperatures which formation of the open structure is dominated, however as shown in Fig. 2 its applicability for high temperatures is reasonable. On the basis of Eq. (22), the new EOS does not show a correct behavior for the third and higher virial coefficients at low temperatures, due to the fact that formations of such clusters are discarded in the model used to derive the EOS.

Acknowledgements

We would like to thank to the Sharif University of Technology research council for financial support.

References

[1] G.A. Parsafar, E.A. Mason, J. Phys. Chem. 97 (1993) 9048.
[2] E. Keshavarzi, G.A. Parsafar, B. Najafi, Int. J. Thermophys. 20 (2) (1999) 651.
[3] E. Keshavarzi, G.A. Parsafar, J. Phys. Chem. B 103 (1999) 6584.
[4] M.H. Ghatee, M. Bahadori, J. Phys. Chem. B 108 (2004) 4141.
[5] J.S. Rowlinson, F.L. Swinton, Liquids and Liquid Mixtures, third ed., Butterworth, London, 1982, pp. PP287–PP288.
[6] G.A. Parsafar, E.A. Mason, J. Phys. Chem. 98 (1994) 1962.
[7] G.A. Parsafar, N. Sohrabi, J. Phys. Chem. 100 (1996) 12644.
[8] B. Najafi, G.A. Parsafar, S. Alavi, J. Phys. Chem. 99 (1995) 9248.
[9] S. Alavi, G.A. Parsafar, B. Najafi, Int. J. Thermophys. 16 (1995) 1421.
[10] G.A. Parsafar, N. Farzi, B. Najafi, Int. J. Thermophys. 18 (1997) 1197.
[11] G.A. Parsafar, J. Sci. Islamic Repub. Iran 2 (1991) 111.
[12] J.A. Barker, D.H. Henderson, J. Chem. Phys. 47 (1967) 2856; J.A. Barker, D.H. Henderson, J. Chem. Phys. 47 (1967) 4717.
[13] J.D. Weeks, D. Chandler, J. Chem. Phys. 54 (12) (1971) 5237.
[14] H. Andersen, J.D. Weeks, D. Chandler, Phys. Rev. A 4 (4) (1971) 1597.
[15] D. Chandler, J.D. Weeks, Phys. Rev. Lett. 25 (1970) 149.
[16] D. Ben-Amotz, G. Stell, J. Phys. Chem. B 108 (2004) 6877.
[17] T.W. Melnyk, W.R. Smith, Mol. Phys. 40 (2) (1980) 317.
[18] I. Nezbeda, W.R. Smith, Chem. Lett. Phys. 64 (1) (1979) 146.
[19] R.W. Zwanzig, J. Chem. Phys. 22 (1954) 1420.
[20] F.H. Stillinger, H. Sakai, S. Torqato, J. Chem. Phys. 17 (1) (2002) 288.
[21] E.K. Goharshadi, A. Morsali, M. Abbaspour, Fluid Phase Equilib. 230 (2005) 170.
[22] S. Hess, Physica A 267 (1999) 58.
[23] D.R. Fernando, G. Stell, D. Ben-Amotz, J. Phys. Conden. Matter 16 (2004) S4887.
[24] J.P. Hsu, D. Chandler, L.J. Lowden, Chem. Phys. 14 (1976) 213.
[25] F. Carnahan, K.E. Starling, J. Chem. Phys. 51 (1969) 635.
[26] R. Dohrn, J.M. Prausnitz, Fluid Phase Equilib. 61 (1990) 53.
[27] D.M. Heyes, J. Chem. Phys. 107 (6) (1997) 1963.
[28] L. Boltzmann, Lectures on Gas Theory, University of California Press, Berkeley, CA, 1964.
[29] G. Soave, Chem. Eng. Sci. 27 (1972) 1197.
[30] D. Deiters, Chem. Eng. Sci. 36 (1981) 1139.
[31] E.W. Lemmon, M.O. Mclinden, M.L. Huber, NIST Standard Reference Database, 23 (2002) Version 7.0.
[32] NIST Chemistry Webbook, http://www.webbook (Nat. Inst. Stds. Technol., Gaithersburg, Maryland, 2006).
[33] P.H. Pool, F. Sciortino, T. Grande, H.E. Stanley, C.A. Angell, Phys. Rev. Lett. 73 (1994) 1632.
[34] C.A. Jeffery, P.H. Austin, J. Chem. Phys. 110 (1) (1999) 484.
[35] D. Ben-Amotz, G. Stell, J. Chem. Phys. 119 (20) (2003) 10777.
[36] J.O. Hirshfelder, C.F. Curtiss, R.B. Bird, Molecular Theory of Gas and Liquids, John Wiley & Sons, 1964. (a) Appendix I-A, p. 1111; (b) pp. 296–298.
[37] G.A. Parsafar, H. Saydi, Int. J. Thermophys. 25 (6) (2004) 1819.
[38] G.A. Parsafar, F. Kermanpour, B. Najafi, J. Chem. Phys. 103 (1999) 7287.
[39] A. Boushehri, F.-M. Tao, E.A. Mason, J. Chem. Phys. 97 (1993) 2711.
[40] G.A. Parsafar, M. Khanpour, A.A. Mohammadi, Chem. Phys. 326 (2006) 527.
[41] G.A. Parsafar, M. Shokouhi, Mol. Phys. 104 (20–21) (2006) 3269.
[42] E.A. Mason, T.H. Spurling, The Virial Equation of State, Pergamon, Oxford, 1969 (Section 2.9).
[43] J.A. Beattie, W.H. Stockmayer, Rep. Prog. Phys. 7 (1940) 195.
[44] Y. Song, E.A. Mason, J. Chem. Phys. 91 (12) (1989) 7840.
[45] D.G. Miller, Ind. Eng. Chem. Fundam. 9 (1970) 585.
[46] G.A. Parsafar, C. Izanloo, Int. J. Thermophys. 27 (5) (2006) 1564.
[47] R.D. Gunn, P.L. Chueh, J.M. Prausnitz, Cryogenics 6 (1966) 324.
[48] G.W. Dilay, R.A. Heidemann, Ind. Eng. Chem. Fundam. 25 (1986) 152.
[49] H.B. Callen, Thermodynamics and an Introduction to Thermodynamics, John & Sons, 1985 (Chapter 8).
[50] A. Michels, J.M. Levelt, W. de Graaff, Physica xxIV (1958) 659.